

## Hydrogen-bonded semiconducting pigments for air-stable field-effect transistors

By *Eric Daniel Głowacki\**, *Mihai Irimia-Vladu*, *Martin Kaltenbrunner*, *Jacek Gąsiorowski*, *Matthew S. White*, *Uwe Monkowius*, *Giuseppe Romanazzi*, *Gian Paolo Suranna*, *Piero Mastrorilli*, *Tsuyoshi Sekitani*, *Siegfried Bauer*, *Takao Someya*, *Luisa Torsi*, and *Niyazi Serdar Sariciftci*

[\*]Eric Daniel Głowacki, Dr. Mihai Irimia-Vladu, Jacek Gąsiorowski, Dr. Matthew White, Prof. Niyazi Serdar Sariciftci  
Linz Institute for Organic Solar Cells (LIOS), Physical Chemistry  
Johannes Kepler University  
Altenbergerstrasse 69, Linz 4040 Austria  
E-mail: eric\_daniel.glowacki@jku.at

Dr. Mihai Irimia-Vladu, Dr. Martin Kaltenbrunner, Prof. Siegfried Bauer  
Soft Matter Physics,  
Johannes Kepler University  
Altenbergerstrasse 69, Linz 4040 Austria

Dr. Martin Kaltenbrunner, Dr. Tsuyoshi Sekitani, Prof. Takao Someya  
Department of Electrical and Electronic Engineering and Information Systems, The  
University of Tokyo, 7-3-1 Hongo, Bunkyo-ku, Tokyo 113-8656, Japan

Dr. Martin Kaltenbrunner, Dr. Tsuyoshi Sekitani, Prof. Takao Someya  
Exploratory Research for Advanced Technology (ERATO), Japan Science and Technology  
Agency (JST), 2-11-16, Yayoi, Bunkyo-ku, Tokyo 113-0032, Japan

Dr. Uwe Monkowius  
Institute of Inorganic Chemistry,  
Johannes Kepler University  
Altenbergerstrasse 69, Linz 4040 Austria

Dr. Giuseppe Romanazzi, Dr. Gian Paolo Suranna, Prof. Piero Mastrorilli  
Dipartimento di Ingegneria Civile, per l'Ambiente e il Territorio, Edile e di Chimica  
(DICATECh), Politecnico di Bari, Via Orabona 4, 70125 Bari, Italy

Prof. Luisa Torsi  
Dipartimento di Chimica, Università degli Studi di Bari, 70126 Bari, Italy

Keywords: organic electronics, organic pigments, field-effect transistors

Progress in the field of organic electronics continues to enable novel electronic technologies, in large part propelled by the development of new, high-performance organic semiconductors. Optimum materials must combine low cost, high charge carrier mobility, and stable operation in air. A high degree of intramolecular  $\pi$ -conjugation and close intermolecular stacking are considered to be necessary for good charge transport. In this paper, we investigate low-cost hydrogen-bonded organic molecules primarily used as toners in inkjet printing. Though these

molecules have limited intramolecular conjugation, in the aggregated pigment form they show high carrier mobility up to  $1.5 \text{ cm}^2/\text{Vs}$  in organic field-effect transistors; with on-off ratios up to  $5 \times 10^6$ . The transistors are stable under operation in air without significant degradation for at least 140 days. We thereby demonstrate that maximizing intramolecular  $\pi$ -conjugation may not be requisite for high performance, and that intermolecular hydrogen-bonding may be utilized in the design of air-stable, low-cost organic semiconductors.

In recent years organic electronics evolved into a multibillion dollar industry. Organic semiconductors and conductors enable technologies<sup>[1, 2]</sup> remarkable for low weight, flexibility<sup>[3]</sup> and stretchability.<sup>[4]</sup> Ideally, organic electronic devices can be mass-produced with minimal cost and ecological impact.<sup>[5]</sup> Synthesis of novel materials with desired properties is the most successful approach towards achieving this goal. In the quest for optimum organic semiconductors, molecular design focuses on planar molecules with  $\text{sp}^2$  hybridized carbons to afford  $\pi$ -conjugated systems.<sup>[6,7]</sup> Though organic materials are nearly unlimited in chemical design, this focus on  $\pi$ -conjugation significantly narrows the available molecular library. The pigments presented in this work represent one class of materials that would fall outside of this selection rule.

Toner pigments used in inkjet printing are stable in air and available at low cost. They often possess carbonyl or amine groups in conjugated segments, and form intermolecularly H-bonded organic solids with high lattice energies. As organic semiconductors, amine/carbonyl dye molecules were reported to support only very low field-effect charge carrier mobilities in the  $1 \times 10^{-7} - 5 \times 10^{-4} \text{ cm}^2/\text{Vs}$  range.<sup>[8,9,10]</sup> Here we show significantly improved field-effect mobilities between 0.2 and  $1.5 \text{ cm}^2/\text{Vs}$  in the H-bonded analogs of tetracene and pentacene. Furthermore, we report stable operation of field-effect transistors in air without strong performance degradation for over 140 days. Our results may stimulate further experimental work to elucidate the potential of intermolecular H-bonding in the design of organic semiconductors and may motivate theoretical and experimental studies of the solid state structure and charge carrier transport mechanism in such materials.

Learning from nature was a strong motivation for this work. Many stable dyes and pigments of natural origin are based on hydrogen-bonded  $\pi$ -stacked organic solids.<sup>[11]</sup> An example is the indigo family, and indeed we recently observed ambipolar charge transport in indigoids with mobilities in the range of  $1 \times 10^{-2} - 0.4 \text{ cm}^2/\text{Vs}$ .<sup>[12,13,14]</sup> Here we investigate the charge

transport in the five-ring quinacridone and the four-ring epindolidione shown in **Figure 1a**, the hydrogen-bonded analogs of the well-known organic semiconductors pentacene and tetracene. Industrially, quinacridone nanocrystallites form the magenta toner widely used in inkjet printers (available commercially for ~\$0.50/kg). Epindolidione is a related yellow colorant also currently marketed in ink formulations for inkjet printing.<sup>[15]</sup> These molecules are nontoxic and commonly found in household paints and cosmetics.<sup>[11]</sup> We compare these pigments side-by-side with pentacene and tetracene and show air-stable charge transport in organic field-effect transistors (OFETs), while the performance of pentacene and tetracene transistors degrades within a few days.

From a chemical perspective, resonance structures of molecules like epindolidione and quinacridone featuring enol or imine character are thermodynamically unfavorable under neutral pH conditions; therefore the carbonyl and amine groups essentially perturb conjugation.<sup>[6,7]</sup> From such a perspective, molecules with carbonyl and amine groups can be regarded as being less conjugated than the acenes. However, these molecules have intermolecular H-bonding between carbonyl and amine groups on adjacent molecules. The molecules strongly aggregate and form pigment particles with markedly different optical properties in comparison to isolated molecules. This shift is illustrated in **Figure 1b**, where solutions of the dyes are shown alongside aggregated solid pigment powders. For example, quinacridone is pale yellow in dilute solution, but adopts colors ranging from red to purple in the aggregated H-bonded pigment form. UV-Vis absorption spectra of epindolidione and quinacridone in dilute solution and thin films are shown in **Figure 2a and 2b**, respectively. This behavior of becoming highly-colored only in the aggregated state signals the involvement of strong intermolecular electronic coupling.<sup>[16,17,18]</sup> This is also indicated in the high dielectric constant and low exciton binding energy in quinacridone thin films, resulting in high quantum efficiency of photogeneration in quinacridone metal-insulator-metal diodes.<sup>[19]</sup> In order to estimate HOMO and LUMO energies we measured cyclic voltammetry (CV) and UV-Vis absorption of vacuum-evaporated films of each material. The absorption coefficients of thin films of epindolidione and quinacridone are plotted in **Figure 2b**. The estimates for energy levels are presented in **Table 1**. **Figure 2c** shows the CV scans of epindolidione and quinacridone. The CV measurements demonstrate that both materials support reversible two-electron oxidation and reduction. We carried out DFT calculations to better understand the properties of the molecules.<sup>[20]</sup> Relative calculated energy levels are shown in **Figure 3**. The LUMO levels of the acenes and their H-bonded analogs do not differ

significantly. The incorporation of the heteroatoms in the structures of epindolidione and quinacridone results in significantly more-stable HOMO levels relative to the acenes, however. This gives a larger HOMO-LUMO gap and helps to explain the blue-shifted absorption of the H-bonded molecules relative to the acenes; while the deeper HOMO levels correlate with the better air stability. These findings correspond well to the experimental CV data. Due to H-bonding in the solid state, epindolidione or quinacridone molecules can be regarded as mutually protonating and deprotonating one another, leading to a situation where the enol and imine mesomers are more favored.<sup>[21]</sup> An interesting experimental observation is that quinacridone dissolved in concentrated H<sub>2</sub>SO<sub>4</sub> becomes blue, with an absorption spectrum very similar to that of pentacene, indicating that the protonated form indeed features an enol-imminium aromatic backbone.<sup>[22]</sup> We conducted calculations on the protonated molecules, finding that in the case of epindolidione and quinacridone both HOMO and LUMO levels become more stable and the gap shrinks. This is shown in **Figure 3**. This suggests that intermolecular H-bonding interactions support mesomeric structures with increased conjugated character. To support charge transport in solid films, organic molecules must demonstrate  $\pi$ -stacking. It is known that quinacridone and related H-bonded materials such as the indigos show relatively tight  $\pi$ -stacking along one crystallographic direction. In all four of the reported polymorphs of quinacridone, the  $\pi$ -stacking distance is found to be  $\sim 3.4\text{\AA}$ . Based on the evidence of film color,<sup>[16]</sup> growth temperature,<sup>[23]</sup> and IR absorption<sup>[24]</sup> we conclude that quinacridone arranges in the  $\beta$  polymorph in the transistors discussed in this paper. Since it is known that quinacridone adopts tight  $\pi$ -stacking along one crystallographic direction, controlling orientation of molecules in the film is crucial to obtain good transport in a device.<sup>[25]</sup> For this reason we choose to use low surface energy hydrophobic gate dielectric surfaces to achieve ‘standing up’ molecules and thus  $\pi$ -stacking parallel to the gate electrode, perpendicular to the source and drain contacts.<sup>[12,13,19]</sup> We were not able to, despite extensive efforts, obtain single crystal x-ray diffraction data for epindolidione. The difficulties in establishing crystal structure in this class of materials have been reviewed.<sup>[16,26]</sup>

To compare the strength of intermolecular interactions in the van der Waals acenes versus the H-bonded analogs we conducted thermogravimetric analysis (TGA). Epindolidione and quinacridone sublimed at 400 °C and 535 °C, respectively, versus 280°C and 370°C for tetracene and pentacene. The difference in molecular weight between the acenes and their analogous H-bonded molecules is insignificant, but the sublimation temperature is much

higher for the materials with strong intermolecular interactions. The TGA measurement details and results are shown as figure S1 in the supplementary information.

OFET devices were fabricated using a bottom gate / top contact configuration, with channel dimensions of  $W/L = 5 \text{ mm} / 40 \text{ }\mu\text{m}$ . Electrochemically-grown  $\text{Al}_2\text{O}_3$  (32 nm) passivated by vacuum-evaporated tetratetracontane, ( $\text{C}_{44}\text{H}_{90}$ , TTC) served as the gate dielectric. H-bonded pigments have been previously tested in OFET configurations on  $\text{SiO}_2$  gate dielectrics and the resulting mobilities were poor, in the range  $1 \times 10^{-7} - 5 \times 10^{-4} \text{ cm}^2/\text{Vs}$ .<sup>[8,9]</sup> The low surface energy of the aliphatic TTC is critical for the growth orientation of the H-bonded molecules, providing  $\pi$ -stacking parallel to the gate electrode and therefore high mobilities.<sup>[12,13,19]</sup> The favorable properties of TTC have been reported in other small molecule semiconductors as well.<sup>[27,28]</sup> The mobility values are summarized in **Table 1**. All devices were stored and measured in ambient air under standard laboratory fluorescent lamp lighting unless otherwise noted. With gold source and drain electrodes, pentacene showed characteristic performance<sup>[29]</sup> with hole mobilities of  $\sim 1 \text{ cm}^2/\text{Vs}$  and electron mobilities of  $0.2 \text{ cm}^2/\text{Vs}$  (the latter measured only in  $\text{N}_2$  atmosphere). Tetracene likewise afforded mobilities consistent with literature reports<sup>[30]</sup>, approx.  $0.1 \text{ cm}^2/\text{Vs}$  for holes. The transfer and output characteristics of these ‘standard’ devices are shown in the supplementary information, S2. Epindolidione OFET transfer curves measured in air on day 1 and on day 100 are shown in **Figure 4a** and **Figure 4c**, respectively. Output characteristics are shown in supplementary information figure S3. This material demonstrated mobilities in the range of  $0.9 - 1.5 \text{ cm}^2/\text{Vs}$  for holes, and was thus on par with pentacene. With on/off ratio of  $\sim 10^7$  and negligible hysteresis these devices are superior to the pentacene OFETs that we fabricated. The devices demonstrated air stability with on/off ratio and threshold voltage hardly changing after 100 days. Transfer characteristics for quinacridone OFETs measured in air on day 1 and on day 100 are shown in **Figure 4b** and **Figure 4d**, respectively. Output characteristics are shown in supplementary information figure S4. Quinacridone performed with mobilities of around  $0.2 \text{ cm}^2/\text{Vs}$ . The operational stability in air was comparably impressive, with threshold voltage remaining stable. The devices, however, showed a decline in on/off ratio. The mobility and On/Off ratio values for the OFETs as a function of time are shown in **Figure 4e,f**. These are the averaged results of a 140-day stability study where a dozen transistors of each material were stored and measured in air. It was found that the H-bonded materials show excellent operational stability relative to their acene counterparts. While both pentacene and tetracene hole mobility and on/off ratio each deteriorate by two orders of magnitude after several days in air, these values

for epindolidione and quinacridone degrade by ~20% over the time period of 140 days. Epindolidione mobility degrades with a  $T_{80}$  lifetime (time to decay to 80% of the initial value) of ~85 days, whereas quinacridone demonstrates  $T_{80}$  of ~115 days. **Figure 5** shows a summary of  $T_{80}$  values versus mobility for a number of hole-transporting materials in OFET devices reported between 2008-2012 with epindolidione and quinacridone shown for comparison. The H-bonded pigments compare favorably with stability studies of state-of-the-art ‘air-stable’ p-type devices. [31,32,33,34,35,36,37,38,39,40,41,42] We have not conducted stability studies for n-channel operation, which, due to the high-lying LUMO level should not be possible in air for epindolidione and quinacridone. Appropriate synthetic modification of derivatives, according to recent progress in designing air-stable electron-transporting materials, may result in stable ambipolar transport.<sup>[43,44]</sup>

To rationalize the difference in mobility between epindolidione and quinacridone we speculate that crystallite grain size, *i.e.* intergrain resistance, may play the limiting role. From atomic-force microscopy (AFM), we consistently found that epindolidione films were composed of grains of significantly larger size than quinacridone. AFM scans of both materials deposited on  $\text{Al}_2\text{O}_3/\text{TTC}$  are shown in **Figure 6a,b**. Quinacridone films consisted of rod-shaped crystallites 100-200 nm in size. Epindolidione crystallites, in contrast, were larger, being 400-1000 nm in size. With bigger crystallites, the decrease in the number of grain boundaries may account for the higher observed mobility in epindolidione OFETs.

We found that quinacridone, like the structurally-related indigoids,<sup>[12,13]</sup> supports ambipolar transport. In  $\text{N}_2$  environment, with silver source/drain contacts, quinacridone demonstrates ambipolar transport with effective carrier mobility of  $\sim 0.01 \text{ cm}^2/\text{Vs}$  for both carriers. The transfer and output characteristics for such a device are shown in supplementary figure S5. Due to this well-balanced ambipolarity, we measured simple voltage inverter circuits demonstrating competitive gains in the 100-200 range using quinacridone OFETs, with output characteristics shown in supplementary figure S6.

This study compares two of the most well-known organic semiconductors to their H-bonded analogs. The results suggest that intermolecular H-bonded pigments support air stable charge carrier transport with high mobility. By demonstrating air-stability and good electronic performance, we propose that such H-bonded pigments could be an interesting new paradigm for organic semiconductor design, as these molecules structurally fall outside of what is

normally considered for organic semiconductors. Perhaps the same materials used in printer inks and hair-dyes can be used to fabricate future electronic technologies.

## Experimental Section

*Materials:* Quinacridone was obtained from TCI and purified by temperature gradient sublimation using a source temperature of 350 °C, with a vacuum of  $1 \times 10^{-6}$  mbar. We followed the synthetic approach for the preparation of epindolidione reported by Jaffe and Matrick [45], although the suggestions of Kemp and co-workers [46] proposed for the preparation of the first three intermediates were also taken into account. Epindolidione was likewise purified by temperature gradient sublimation, using a source temperature of 270 °C.

*Materials characterization:* Thermogravimetric analyses (TGA) were performed under a nitrogen atmosphere (flow of 40 mL min<sup>-1</sup>) with a Perkin-Elmer Pyris 6 TGA in the range from 30 to 800 °C with a heating rate of 10 °C min<sup>-1</sup>. Temperatures at which a 5% weight loss occurred were accepted as the values for sublimation temperature [47]. Cyclic voltammetry (CV) measurements were conducted using 50 nm of the small molecules evaporated on indium tin oxide (ITO) glass serving as the working electrode. A platinum foil was used as the counter electrode, with Ag/AgCl as the reference electrode and 0.1 M tetrabutylammonium hexafluorophosphate in acetonitrile as the electrolyte. Calculation of HOMO and LUMO orbitals was done using ferrocene as an external standard, accepting +0.24 V as the formal potential vs. NHE [48] and 4.75 eV [49] as the value of the normal hydrogen electrode (NHE) on the Fermi scale. UV-Vis spectra were obtained using a Cary UV-Vis spectrometer. AFM studies were performed using a Digital Instruments DIMENSION 3100 in tapping mode. A Bruker Dektak profilometer was used to verify thin films thicknesses. A Novocontrol Alpha Analyzer was used to measure frequency-dependent capacitance of the gate dielectrics used in OFETs.

*OFET devices:* OFETs were fabricated on glass slides cleaned sequentially with acetone, isopropanol, detergent, DI water, and O<sub>2</sub> plasma. 100 nm of Aluminum were evaporated through a shadow mask to make the gate electrode. 32 nm of Aluminum Oxide (Al<sub>2</sub>O<sub>3</sub>) was then grown electrochemically [50]. Next, ~20 nm of the oligoethylene TTC (tetratetracontane, C<sub>44</sub>H<sub>90</sub>) [27, 28] was evaporated at a pressure of  $1 \times 10^{-6}$  mbar and subsequently annealed at 60°C for ~12h under nitrogen, creating an inorganic/organic composite gate dielectric with a C<sub>0d</sub> of ~70 nF/cm<sup>2</sup>. The semiconducting layer was vacuum-evaporated at a pressure of  $1 \times 10^{-6}$  mbar with a rate of 0.1 Å/s to a thickness of about 40 nm, except for tetracene [30] which

performed more optimally with faster rates of 4 Å/s. Finally, source and drain contacts were evaporated through a shadow mask resulting in channel dimensions of  $W/L = 5 \text{ nm}/40\mu\text{m}$ . Thicknesses were verified via profilometry measurements and atomic force microscopy.

### Acknowledgements

This work was partially funded by the ERC Advanced Investigators Grant “SoftMap” and the JST-ERATO Someya Bio-Harmonized Electronics grant. Financial support from the city of Linz and the Land Oberösterreich is highly appreciated. We acknowledge funding from The Italian Ministry of Education, University and Research (MIUR) through PRIN project “Electronic and electrochemical biosensors” 2009AZKNJ7. The authors warmly thank Dr. M. Magliulo, L. Leonat, F. Chitanu, M. Dachev, N. Żuchowski, J. Wilkins, M. Scharber, and T. Pho, and the reviewers of this paper for stimulating input.

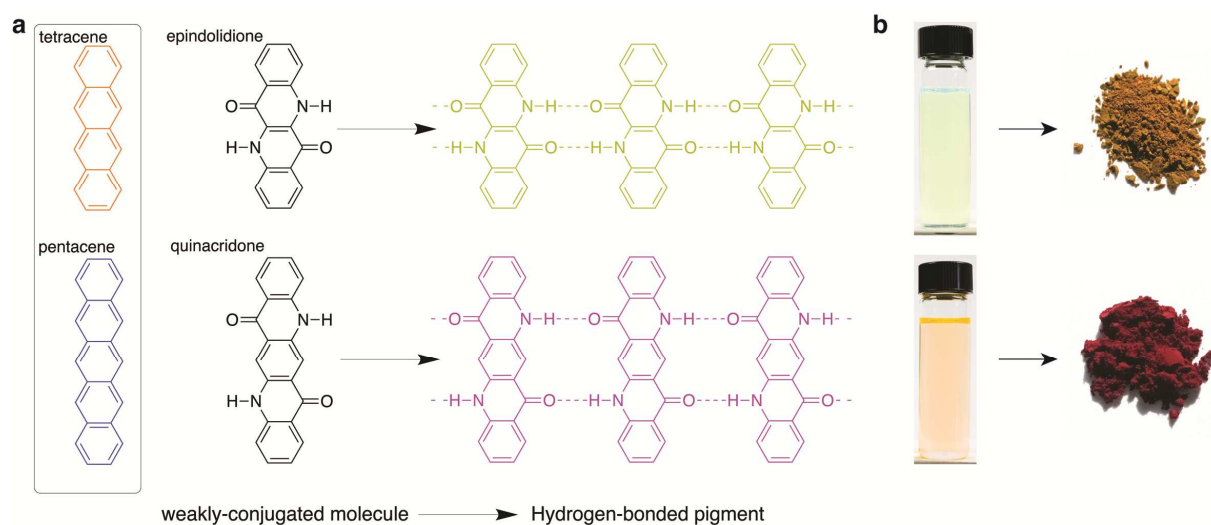


**Figure 1.** H-bonded pigment analogs of the acenes. a) Chemical structures of the acenes: tetracene and pentacene, and their H-bonded analogs: epindolidione and quinacridone. In the solid state, these molecules aggregate into H-bonded pigment particles, which have markedly different optical properties than the isolated dye molecules. Intermolecular hydrogen bonds between carbonyl groups and amine hydrogens are shown with dashed lines. b) 0.1 mM solutions of epindolidione and quinacridone in dimethylsulfoxide. At this concentration the molecules can be dissolved in polar solvents. In the true molecularly-dispersed solution, the isolated chromophores are pale yellow. Upon aggregation in the solid state, a  $\sim 100 \text{ nm}$  bathochromic shift in absorption occurs and they adopt their characteristic pigment colors.

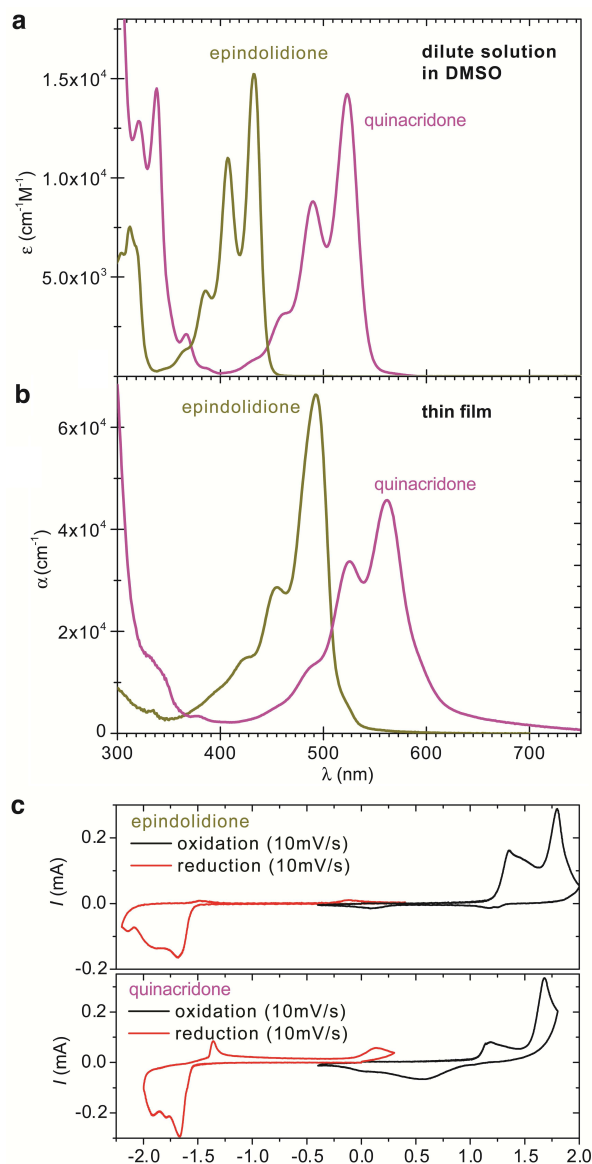


**Figure 2.** Optical and electrochemical properties of H-bonded pigment films. a) Extinction coefficient of epindolidione and quinacridone in DMSO solution. b) Absorption coefficient,  $\alpha$ , of vacuum-evaporated films of epindolidione and quinacridone. c) Cyclic voltammetry scans for epindolidione and quinacridone thin-films evaporated on ITO functioning as the working electrode. Both materials can be reversibly oxidized and reduced.

**Table 1.** Estimated energy levels and mobilities of epindolidione and quinacridone and their acene analogs.

Material	HOMO (eV)	LUMO (eV)	$E_g$ , from CV (eV)	$E_g$ , optical (eV)	Hole mobility, $\mu_h$ (cm <sup>2</sup> /Vs)	Electron mobility, $\mu_e$ (cm <sup>2</sup> /Vs)	Sublimation temperature, from TGA (°C)
tetracene	- 5.3	- 2.8	2.5	2.3	0.1	N/A	280
epindolidione	- 5.5	- 2.9	2.6	2.4	1.5	N/A	404
pentacene	- 5.4	- 3.3	2.1	1.7	1	0.1	370
quinacridone	- 5.5	- 2.9	2.6	2	0.2	0.01	535

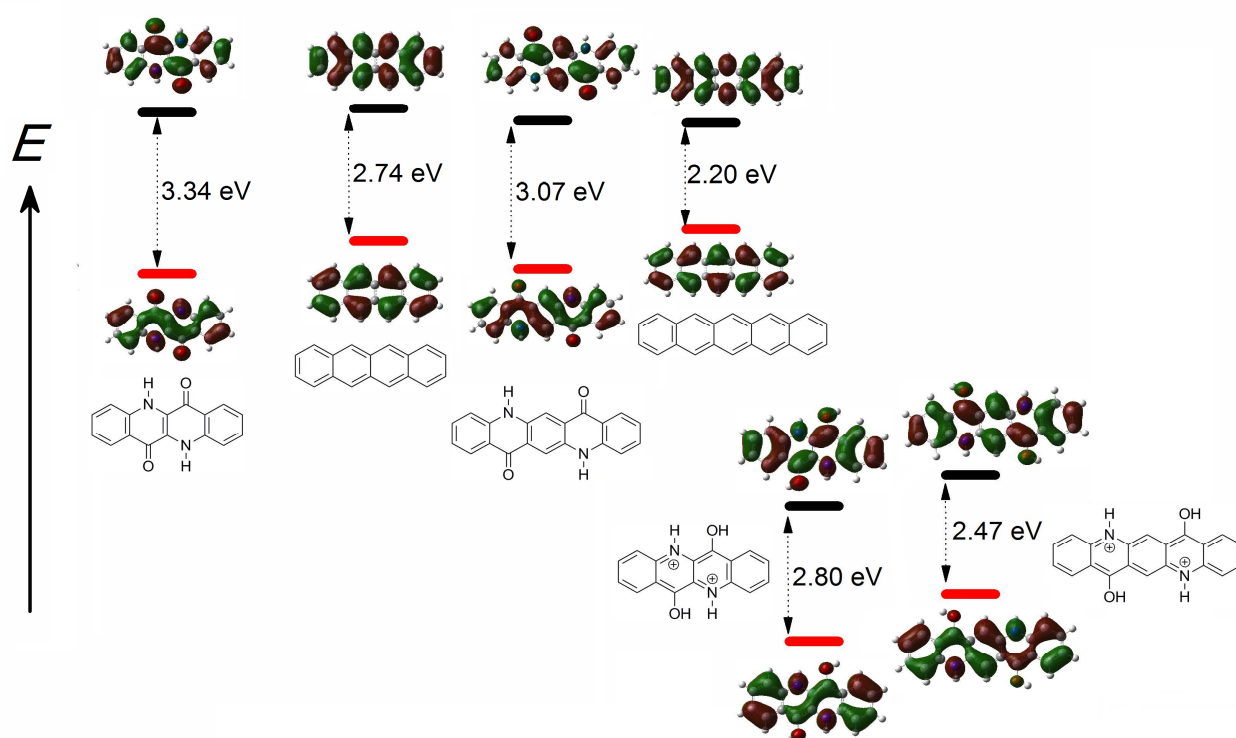


**Figure 3.** Calculated frontier orbitals and relative energy levels from DFT calculations for tetracene and pentacene compared with epindolidione and quinacridone. Calculations for the protonated epindolidione and quinacridone are shown on the right.

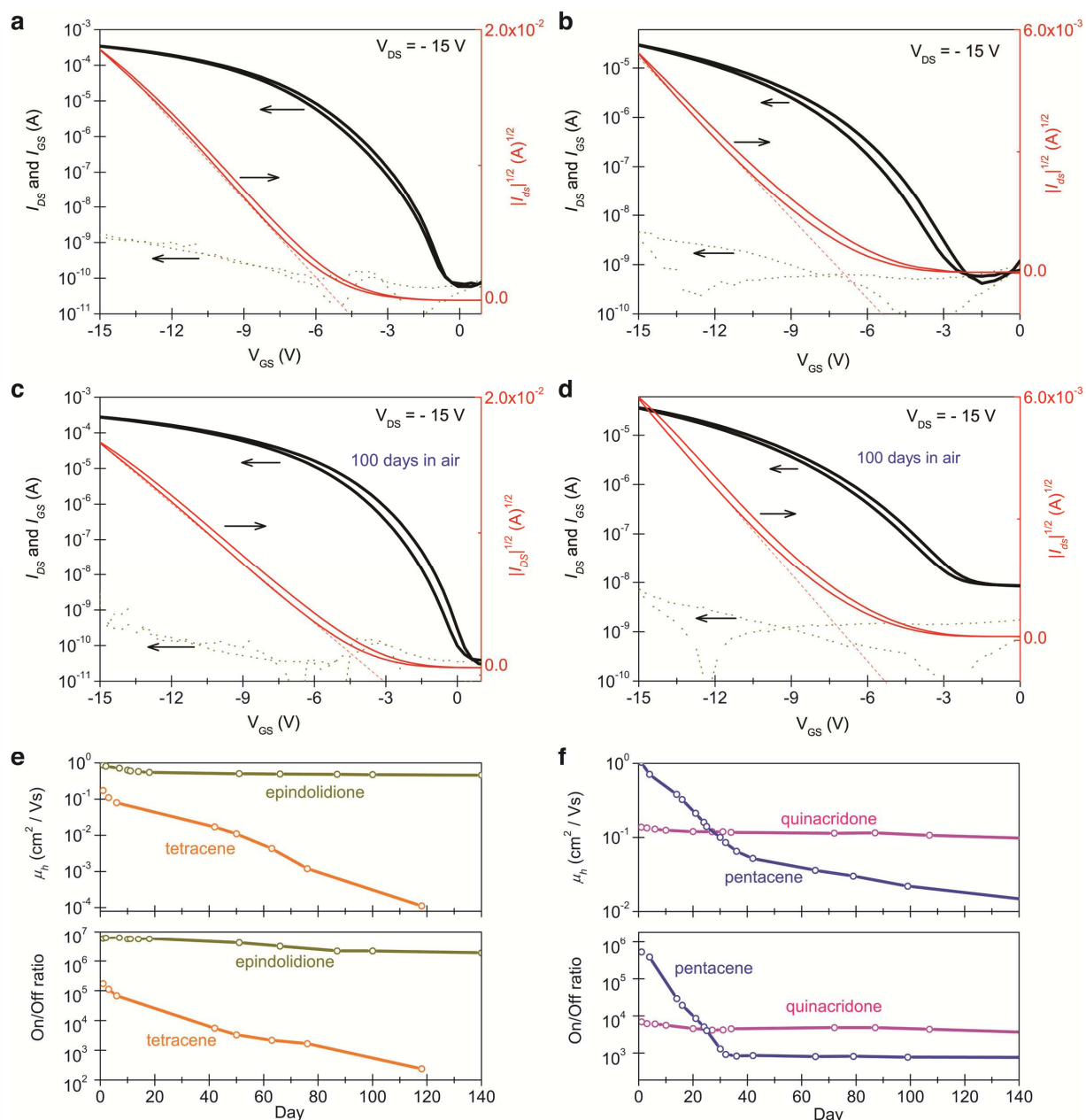


**Figure 4.** H-bonded pigment organic field-effect transistors. a) transfer characteristics of an epindolidione OFET measured in air, (c) transfer characteristics measured after 100 days in air for the same device. b) transfer characteristics of a quinacridone OFET measured in air, (d) transfer characteristics measured after 100 days in air for the same device. e) Comparison of mobility and on/off ratio of epindolidione and tetracene OFETs stored and measured in air over 140 days. f) Mobility and on/off ratio of quinacridone and pentacene OFETs measured over the same period.

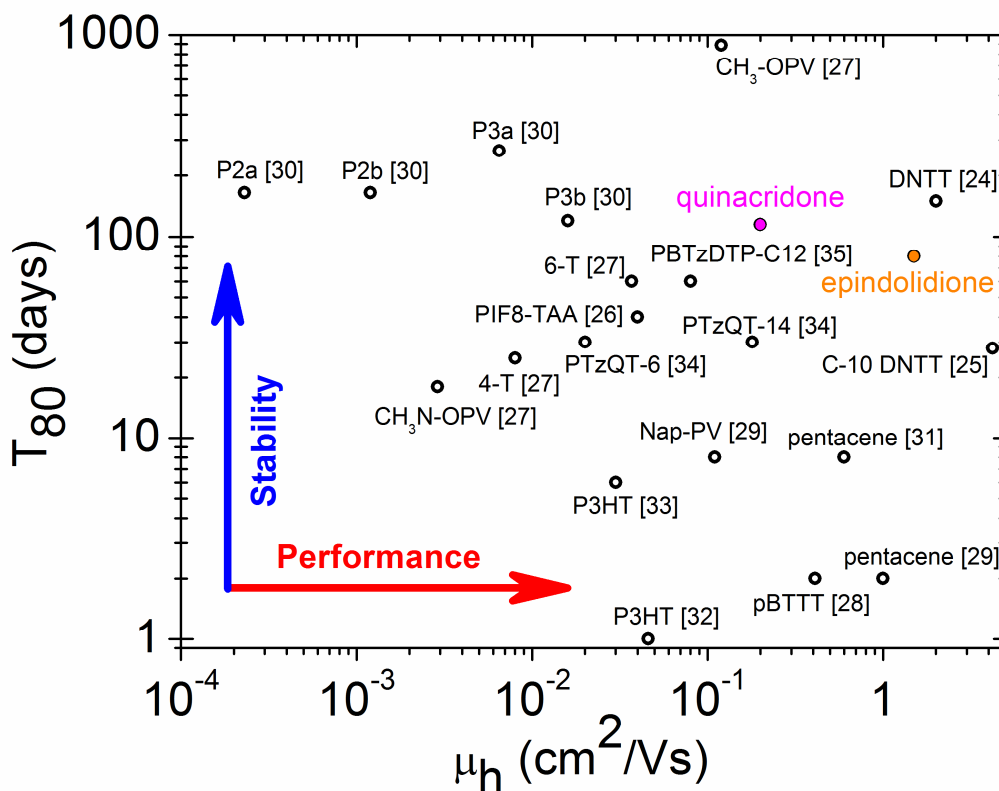


**Figure 5.** Plot of  $T_{80}$  lifetime (time for mobility to degrade to 80% of the initial value) versus initial mobility for a number of reported hole-transporting materials measured in air.

References are shown in brackets next to abbreviated material names.

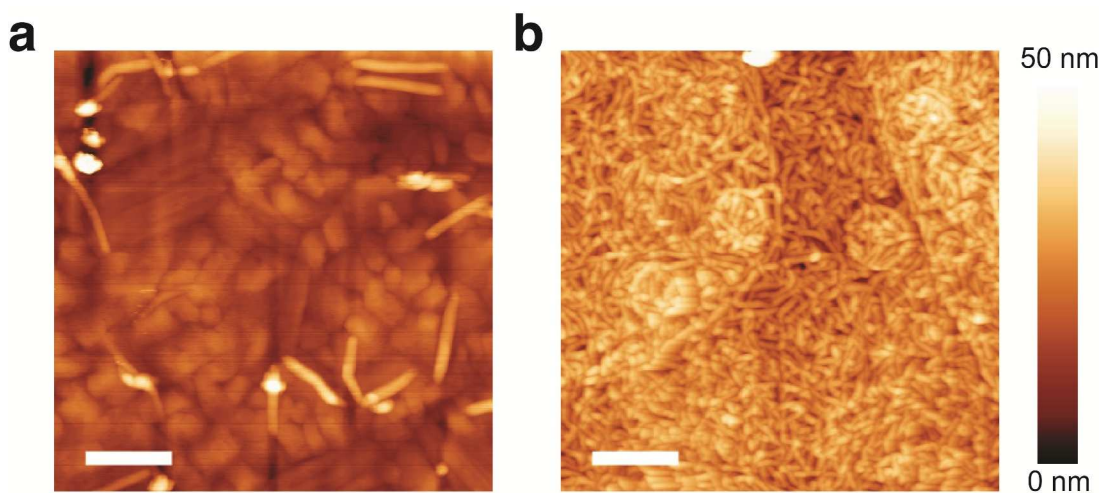


**Figure 6.** AFM images for H-bonded pigment films in OFETs. a) 40 nm of epindolidione on Al<sub>2</sub>O<sub>3</sub>/TTC, and (b) 40 nm of quinacridone on Al<sub>2</sub>O<sub>3</sub>/TTC. Scale bar 500 nm.

## References

- [1] S. R. Forrest, *Nature* **2004**, 428, 911–918.
- [2] M. D. Angione, R. Pilolli, S. Cotrone, M. Magliulo, A. Mallardi, G. Palazzo, L. Sabbatini, D. Fine, A. Dodabalapur, N. Cioffi, L. Torsi, *Mater. Today* **2011**, 14, 424–433.
- [3] T. Sekitani, U. Zschieschang, H. Klauk, T. Someya, *Nat. Mater.* **2010**, 9, 1015–1022.
- [4] M. Kaltenbrunner, M. S. White, E. D. Głowacki, T. Sekitani, T. Someya, N. S. Sariciftci, S. Bauer, *Nat. Commun.* **2012**, 3, 770.
- [5] M. Irimia-Vladu, P. A. Troshin, M. Reisinger, L. Shmygleva, Y. Kanbur, G. Schwabegger, M. Bodea, R. Schwödiauer, A. Mumyatov, J. W. Fergus, V. F. Razumov, H. Sitter, N. S. Sariciftci, S. Bauer, *Adv. Funct. Mater.* **2010**, 20, 4069–4076.
- [6] A. Facchetti, *Chem. Mater.* **2011**, 23, 733–758.
- [7] A. Pron, P. Rannou, *Prog. in Polym. Sci.* **2002**, 27, 135–190.
- [8] H. Yanagisawa, J. Mizuguchi, S. Aramaki, Y. Sakai, *Jpn. J. Appl. Phys.* **2008**, 47, 4728–4731.
- [9] D. Berg, C. Nielinger, W. Mader, M. Sokolowski, *Synt. Met.* **2009**, 159, 2599–2602.
- [10] P. Jonkheijm, N. Stutzmann, Z. Chen, D. M. D. Leeuw, E. W. Meijer, A. P. H. J. Schenning, F. Wu, *J. Amer. Chem. Soc.* **2006**, 128, 9535–9540.
- [11] H. Zollinger, *Color Chemistry: Syntheses, Properties, and Applications of Organic Dyes and pigments*, 3rd ed. (Wiley-VCH, Weinheim, **2003**).
- [12] M. Irimia-Vladu, E. D. Głowacki, P. A. Troshin, G. Schwabegger, L. Leonat, D. K. Susarova, O. Krystal, M. Ullah, Y. Kanbur, M. A. Bodea, V. F. Razumov, H. Sitter, S. Bauer, N. S. Sariciftci, *Adv. Mater.* **2011**, 24, 375–380.
- [13] E. D. Głowacki, L. Leonat, G. Voss, M.-A. Bodea, Z. Bozkurt, A. M. Ramil, M. Irimia-Vladu, S. Bauer, N. S. Sariciftci, *AIP Advances* **2011**, 1, 042132–042137.
- [14] Y. Kanbur, M. Irimia-Vladu, E. D. Głowacki, G. Voss, M. Baumgartner, G. Schwabegger, L. Leonat, M. Ullah, H. Sarica, S. Erten-Ela, R. Schwödiauer, H. Sitter, Z. Küçükyavuz, S. Bauer, N. S. Sariciftci, *Org. Electron.* **2012**, 13, 919–924.
- [15] S. Magdassi, *The Chemistry of Inkjet Inks* (World Scientific Publishing Co. Singapore, **2010**).
- [16] E. F. Paulus, F. J. J. Leusen, M. U. Schmidt, *CrystEngComm* **2007**, 9, 131–143.
- [17] L. Rossi, G. Bongiovanni, A. Borghesi, G. Lanzani, J. Kalinowski, A. Mura, R. Tubino, *Synt. Met.* **1997**, 84, 873–874.
- [18] J. Mizuguchi, T. Senju, *J. Phys. Chem B* **2006**, 110, 19154–19161.
- [19] E. D. Głowacki, L. Leonat, M. Irimia-Vladu, R. Schwödiauer, M. Ullah, H. Sitter, S. Bauer, N. Serdar Sariciftci, *Appl. Phys. Lett.* **2012**, 101, 023305–023308.
- [20] Computational details can be found in the supplementary information file.
- [21] G. Lincke, *Dyes and Pigments* **2002**, 52, 169–181.
- [22] S. S. Labana, L. L. Labana, *Chem. Rev.* **1967**, 67, 1–18.
- [23] N. Nishimura, T. Senju, J. Mizuguchi, *Acta Crystallogr. Sect. E* **2006**, 62, o4683–o4685.
- [24] S. D. Feyter, F. C. D. Schryver, U. Keller, K. Mu, *Chem. Mater.* **2002**, 14, 989–997.
- [25] V. Coropceanu, J. Cornil, D. a da Silva Filho, Y. Olivier, R. Silbey, J.-L. Brédas, *Chem. Rev.* **2007**, 107, 926–952.
- [26] G. Lincke, *Dyes and Pigments* **2000**, 44, 101–122.
- [27] M. Horlet, M. Kraus, W. Brütting, A. Opitz, *Appl. Phys. Lett.* **2011**, 98, 233304–233306.
- [28] A. Opitz, M. Horlet, M. Kiwull, J. Wagner, M. Kraus, W. Brütting, *Org. Electron.* **2012**, 13, 1614–1622.
- [29] T. B. Singh, F. Meghdadi, S. Günes, N. Marjanovic, G. Horowitz, P. Lang, S. Bauer, N. S. Sariciftci, *Adv. Mater.* **2005**, 17, 2315–2320.
- [30] F. Cicoira, C. Santato, F. Dinelli, M. Murgia, M. A. Loi, F. Biscarini, R. Zamboni, P. Heremans, M. Muccini, *Adv. Funct. Mater.* **2005**, 15, 375–380.
- [31] U. Zschieschang, F. Ante, D. Kälblein, T. Yamamoto, K. Takimiya, H. Kuwabara, M. Ikeda, T. Sekitani, T. Someya, J. B.- Nimoth, H. Klauk, *Org. Electron.* **2011**, 12, 1370–1375.
- [32] U. Zschieschang, M. J. Kang, K. Takimiya, T. Sekitani, T. Someya, T. W. Canzler, A. Werner, J. Blochwitz-Nimoth, H. Klauk, *J. Mater. Chem.* **2012**, 22, 4273.
- [33] W. Zhang, J. Smith, R. Hamilton, M. Heeney, J. Kirkpatrick, K. Song, S. E. Watkins, T. Anthopoulos, I. McCulloch, *J. Amer. Chem. Soc.* **2009**, 131, 10814–10815.
- [34] T. Ashimine, T. Yasuda, M. Saito, H. Nakamura, T. Tsutsui, *Jpn. J. Appl. Phys.* **2008**, 47, 1760–1762.
- [35] I. McCulloch, M. Heeney, M. L. Chabinyc, D. DeLongchamp, R. J. Kline, M. Cölle, W. Duffy, D. Fischer, D. Gundlach, B. Hamadani, R. Hamilton, L. Richter, A. Salleo, M. Shkunov, D. Sparrowe, S. Tierney, W. Zhang, *Adv. Mater.* **2009**, 21, 1091–1109.
- [36] H. Nagashima, M. Saito, H. Nakamura, T. Yasuda, T. Tsutsui, *Org. Electron.* **2010**, 11, 658–663.
- [37] X. Guo, R. P. Ortiz, Y. Zheng, Y. Hu, Y.-Y. Noh, K.-J. Baeg, A. Facchetti, T. J. Marks, *J. Amer. Chem. Soc.* **2011**, 133, 1405–18.

- 
- [38] T. Sekitani, T. Someya, *Jpn. J. Appl. Phys.* **2007**, *46*, 4300–4306.
- [39] X. Yu, K. Xiao, J. Chen, N. V. Lavrik, K. Hong, B. G. Sumpter, D. B. Geohegan, *ACS Nano* **2011**, 3559–3567.
- [40] Y. D. Park, D. H. Kim, J. a. Lim, J. H. Cho, Y. Jang, W. H. Lee, J. H. Park, K. Cho, *J. Phys. Chem. C* **2008**, *112*, 1705–1710.
- [41] I. Osaka, R. Zhang, G. Sauvé, D.-M. Smilgies, T. Kowalewski, R. D. McCullough, *J. Amer. Chem. Soc.* **2009**, *131*, 2521–2529.
- [42] J. Liu, R. Zhang, I. Osaka, S. Mishra, A. E. Javier, D.-M. Smilgies, T. Kowalewski, R. D. McCullough, *Adv. Funct. Mater.* **2009**, *19*, 3427–3434.
- [43] C. Piliego, D. Jarzab, G. Gigli, Z. Chen, A. Facchetti, M. A. Loi, *Adv. Mater.* **2009**, *21*, 1573–1576.
- [44] M. Mamada, D. Kumaki, J. Nishida, S. Tokito, Y. Yamashita, *ACS Appl. Mater. Interfaces* **2010**, *2*, 1303–1307.
- [45] E. E. Jaffe, H. Matrick, *J. Org. Chem.* **1968**, *83*, 4004–4010.
- [46] D. S. Kemp, B. R. Bowen, C. C. Muendel, *J. Org. Chem.* **1990**, *55*, 4650–4657.
- [47] T. Okamoto, M. L. Senatore, M.-M. Ling, A. B. Mallik, M. L. Tang, Z. Bao, *Adv. Mater.* **2007**, *19*, 3381–3384.
- [48] C. M. Cardona, W. Li, A. E. Kaifer, D. Stockdale, G. C. Bazan, *Adv. Mater.* **2011**, *23*, 2367–2371.
- [49] D. Baran, A. Balan, S. Celebi, B. Meana-Esteban, H. Neugebauer, N. S. Sariciftci, L. Toppare, *Chem. Mater.* **2010**, *22*, 2978–2987.
- [50] L. A. Majewski, R. Schroeder, M. Grell, *J. Phys. D: Appl. Phys.* **2004**, *37*, 21–24.

---

**Supplementary Information for:**

**Hydrogen-bonded semiconducting pigments for air-stable field-effect transistors**

Eric Daniel Głowacki<sup>1\*</sup>, Mihai Irimia-Vladu<sup>1,2</sup>, Martin Kaltenbrunner<sup>2,3,4</sup>, Jacek Gąsiorowski<sup>1</sup>, Matthew S. White<sup>1</sup>, Uwe Monkowius<sup>5</sup>, Giuseppe Romanazzi<sup>6</sup>, Gian Paolo Suranna<sup>6</sup>, Piero Mastorilli<sup>6</sup>, Tsuyoshi Sekitani<sup>3,4</sup>, Siegfried Bauer<sup>2</sup>, Takao Someya<sup>3,4</sup>, Luisa Torsi<sup>7</sup>, Niyazi Serdar Sariciftci<sup>1</sup>

<sup>1</sup>*Linz Institute for Organic Solar Cells (LIOS), Physical Chemistry, Johannes Kepler University, Altenbergerstrasse 69, Linz 4040 Austria*

<sup>2</sup>*Department of Soft Matter Physics, Johannes Kepler University, Altenbergerstrasse 69, Linz 4040 Austria*

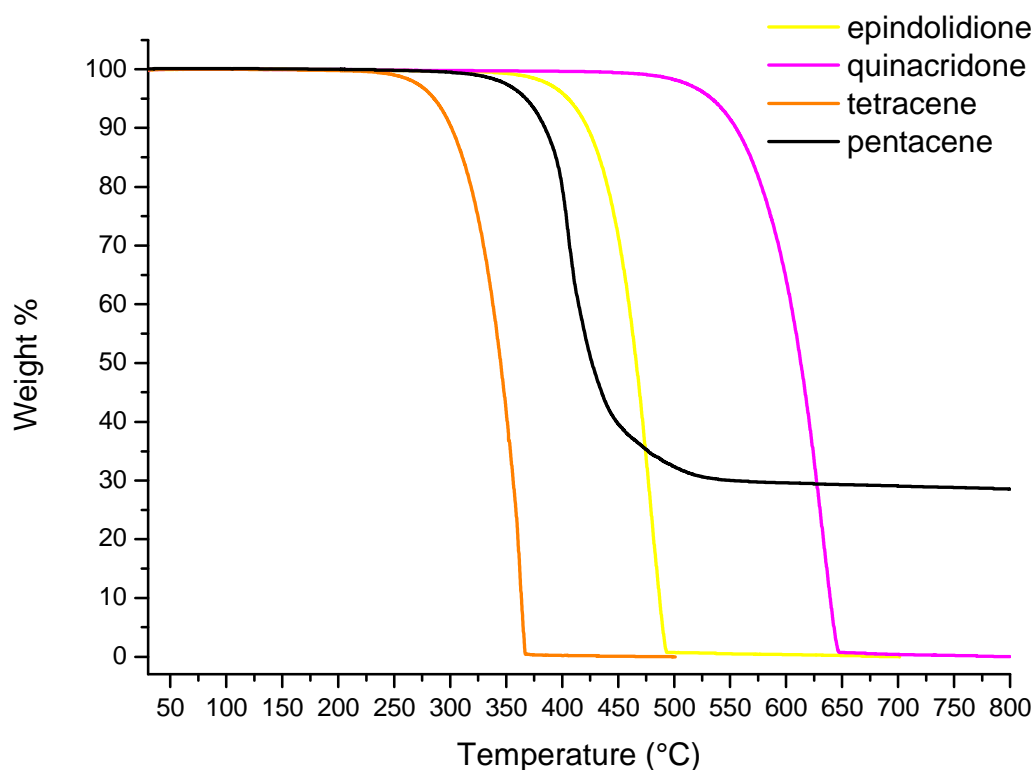
<sup>3</sup>*Department of Electrical and Electronic Engineering and Information Systems, The University of Tokyo, 7-3-1 Hongo, Bunkyo-ku, Tokyo 113-8656, Japan*

<sup>4</sup>*Exploratory Research for Advanced Technology (ERATO), Japan Science and Technology Agency (JST), 2-11-16, Yayoi, Bunkyo-ku, Tokyo 113-0032, Japan*

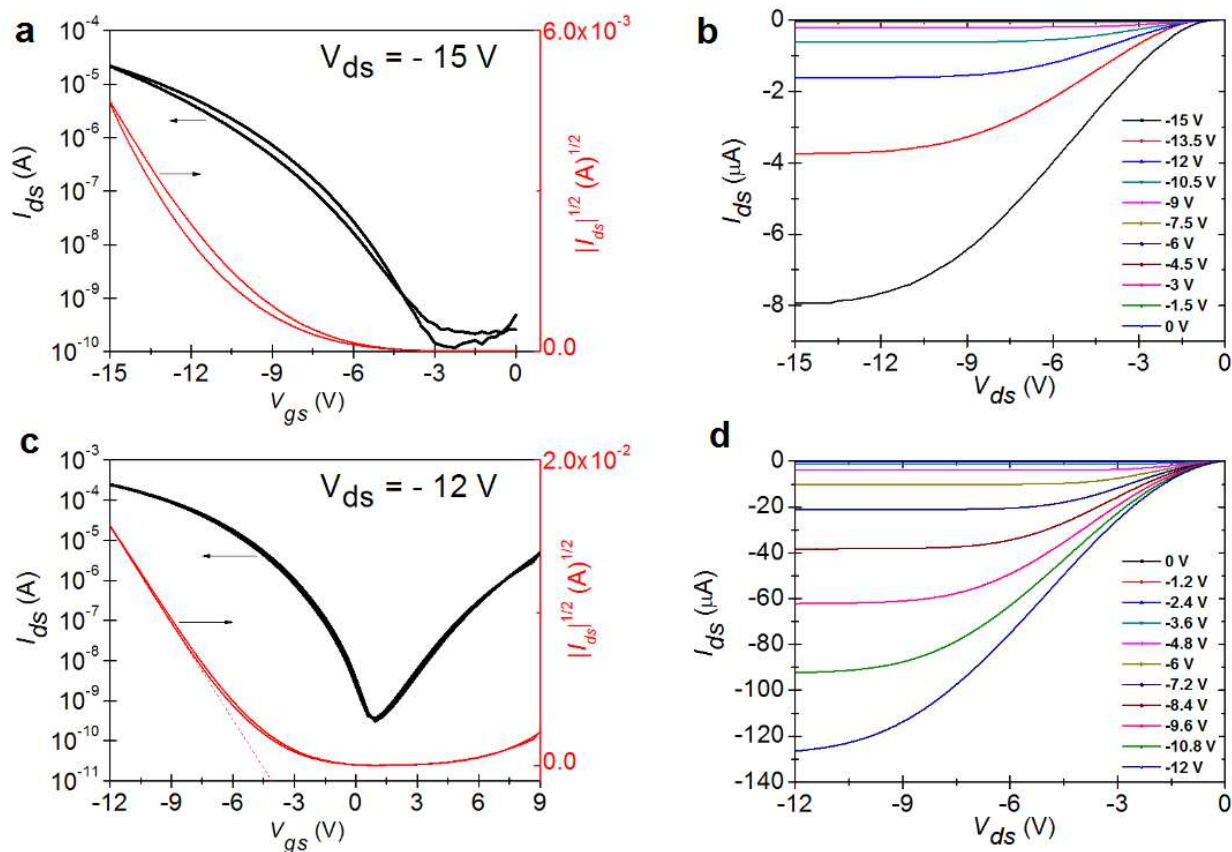
<sup>5</sup>*Institute of Inorganic Chemistry, Johannes Kepler University, Altenbergerstrasse 69, Linz 4040 Austria*

<sup>6</sup>*Dipartimento di Ingegneria Civile, per l'Ambiente e il Territorio, Edile e di Chimica (DICATECh), Politecnico di Bari, Via Orabona 4, 70125 Bari, Italy*

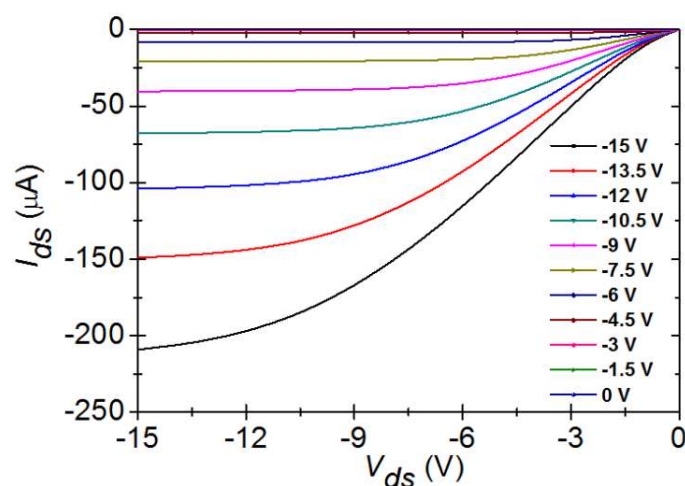
<sup>7</sup>*Dipartimento di Chimica, Università degli Studi di Bari, 70126 Bari, Italy*



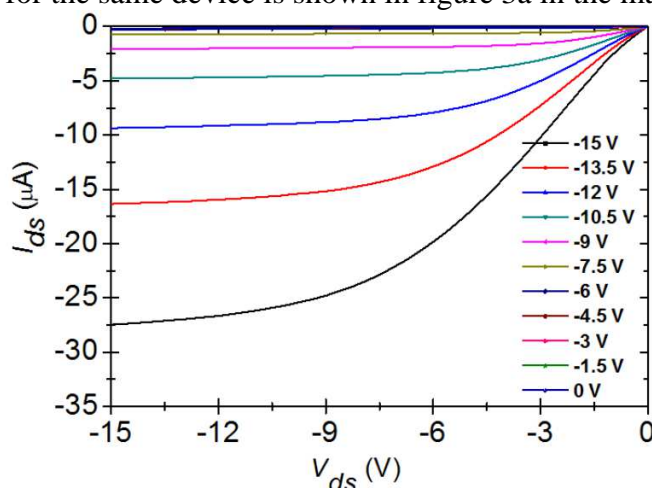
**Supplementary Figure S1.** Thermogravimetric analyses (TGA) for the two acenes and their corresponding H-bonded analogs. TGA scans were performed under a nitrogen atmosphere (flow of 40 mL min<sup>-1</sup>) with a Perkin-Elmer Pyris 6 TGA in the range from 30 to 800 °C with a heating rate of 10 °C min<sup>-1</sup>. All materials sublimed cleaning without leaving charred residue, with the exception of pentacene, which leaves about 30% charred material. This behaviour has been reported before for pentacene by Bao and coworkers [47].



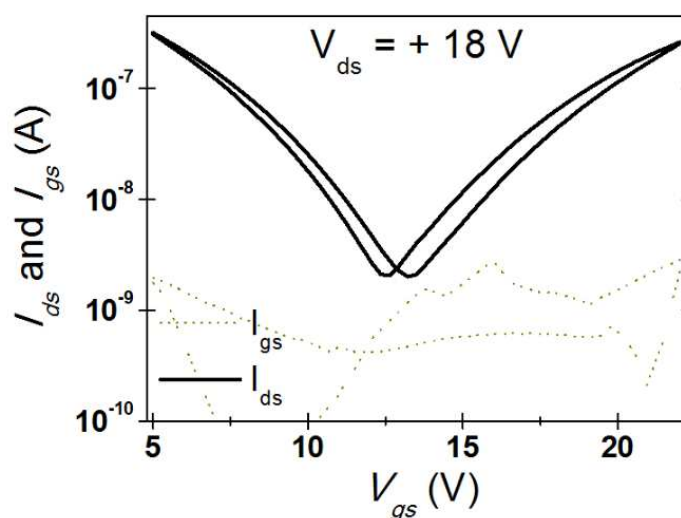
**Supplementary Figure S2.** Tetracene and pentacene OFETs. Tetracene and pentacene OFETs were measured alongside the H-bonded pigments as a point of reference. All devices were fabricated using  $\text{Al}_2\text{O}_3/\text{TTC}$  composite gate dielectric with a  $C_{0d}$  of  $\sim 70$  nF/cm<sup>2</sup>. a) Transfer characteristics for a tetracene OFET, (b) output characteristics for the same device. c) Transfer characteristics for a pentacene OFET measured under  $\text{N}_2$  atmosphere, showing ambipolarity. d) Output characteristics for the same device.



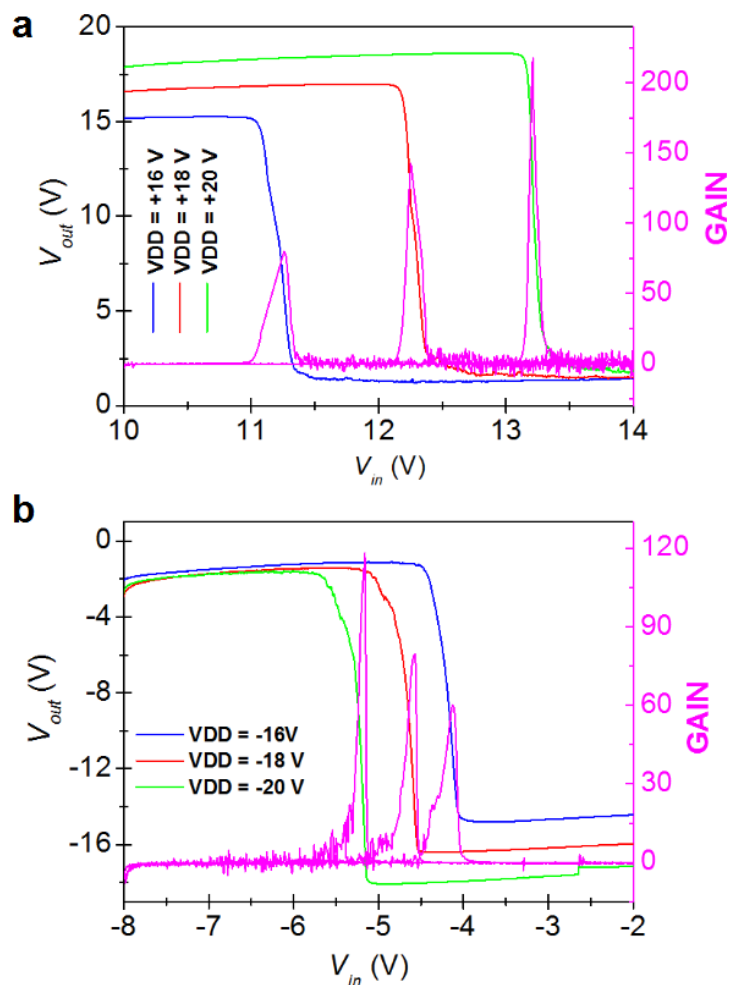
**Supplementary Figure S3.** Output characteristics for an epindolidione OFET. The transfer curve for the same device is shown in figure 3a in the main text.



**Supplementary Figure S4.** Output characteristics for a quinacridone OFET. The transfer curve for the same device is shown in figure 3b in the main text.



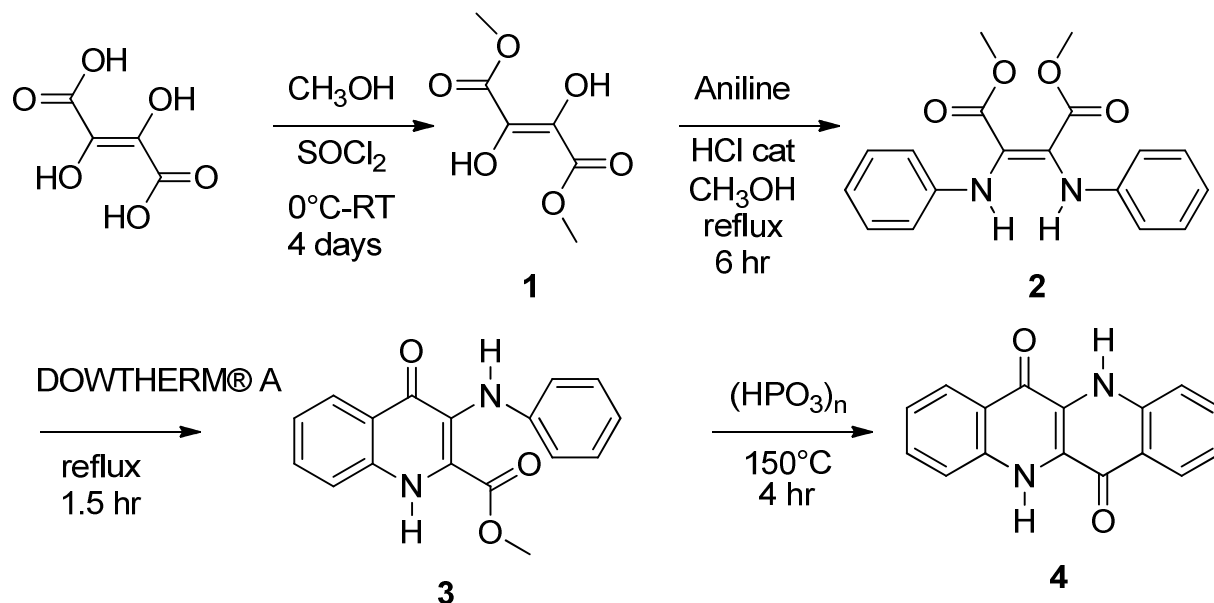
**Supplementary Figure S5.** Transfer characteristics for an ambipolar quinacridone OFET. Silver source/drain electrodes were utilized to support injection of both carriers, the device was measured under  $\text{N}_2$ .



**Supplementary Figure S6.** Quinacridone inverter. Quasi steady-state output characteristics for a voltage inverter based on ambipolar quinacridone OFETs shown in the first quadrant, (a) and the third quadrant, (b).

## Epindolidione synthesis

The synthetic approach (**scheme 1**) for the preparation of epindolidione (*dibenzo[b,g][1,5]naphthyridine-6,12(5H,11H)-dione*) follows the one reported by Jaffe and Matrick, although the suggestions of Kemp and co-workers proposed for the preparation of first three intermediates (**1-3**) were also taken into account [45,46].



Scheme 1

### Computational details:

Gaussian03 program was used in the calculations [51]. Initial coordinates were taken from the corresponding X-ray molecular structure. All quantum-chemical calculations have been carried out using density functional theory (DFT) based method with hybrid B3LYP functional. 6-311+G(d,p) basis has been used through the calculations. The obtained geometries were verified to correspond to a real minimum by establishing an absence of imaginary IR frequencies.

xyz-coordinates of the optimized structures of (absolute energies in Hartrees):

#### - Epindolidione:

C	-4.80040286	-0.92562187	0.00023473
C	-3.57340019	-1.55558460	0.00006365
C	-2.39082004	-0.78761655	-0.00008270
C	-2.47073254	0.62844903	-0.00008928
C	-3.74052831	1.23919823	0.00011202
C	-4.89157806	0.48003570	0.00026757

---

C	-1.25790027	1.44950239	-0.00034482
C	-0.00658737	0.68780116	-0.00023288
C	0.00658737	-0.68780108	-0.00022572
C	1.25790024	-1.44950231	-0.00027647
C	2.47073251	-0.62844902	-0.00006072
C	2.39082008	0.78761656	-0.00006605
H	-5.70458620	-1.52375133	0.00035767
H	-3.50623086	-2.63812557	0.00006203
H	-3.77528504	2.32188904	0.00010448
H	-5.86349607	0.95831360	0.00040380
C	3.74052824	-1.23919828	0.00012040
C	3.57340026	1.55558455	0.00006132
C	4.89157803	-0.48003581	0.00025738
H	5.86349601	-0.95831376	0.00038334
C	4.80040290	0.92562177	0.00022088
H	5.70458625	1.52375119	0.00032760
H	3.77528492	-2.32188910	0.00012195
H	3.50623098	2.63812553	0.00004928
N	-1.16148016	-1.39557132	-0.00018952
H	-1.05850117	-2.40446839	-0.00020023
O	-1.23760988	2.68420118	0.00011054
O	1.23760983	-2.68420112	0.00007088
N	1.16148021	1.39557140	-0.00018188
H	1.05850124	2.40446847	-0.00021736

Total Energy: E = -875.96518453

- **Protonated epindolidione [epiH<sub>2</sub>]<sup>2+</sup>:**

C	4.77156089	-0.98416913	0.00019943
C	3.54297551	-1.60042189	0.00010446
C	2.37597980	-0.81293096	-0.00001774
C	2.46889962	0.62317730	-0.00011100
C	3.76450769	1.21654318	-0.00020945
C	4.88562709	0.43180400	-0.00005282
C	1.27714463	1.36986494	0.00010417
C	0.01898720	0.69997528	0.00003276
C	-0.01898737	-0.69997521	-0.00004175
C	-1.27714455	-1.36986473	-0.00011637
C	-2.46889981	-0.62317751	0.00010571
C	-2.37598007	0.81293075	0.00001382
H	5.67124227	-1.58829707	0.00045444
H	3.46524942	-2.68177973	0.00008202
H	3.88057240	2.29459348	-0.00059825
H	5.86810774	0.88702899	-0.00018610
C	-3.76450791	-1.21654335	0.00021240
C	-3.54297579	1.60042164	-0.00010278
C	-4.88562731	-0.43180422	0.00006172
H	-5.86810795	-0.88702920	0.00020030
C	-4.77156116	0.98416884	-0.00019138
H	-5.67124264	1.58829666	-0.00044107
H	-3.88057284	-2.29459369	0.00060194
H	-3.46524981	2.68177950	-0.00008056
N	1.14512016	-1.40156393	-0.00021691

---

H	1.08280875	-2.41628517	0.00004842
N	-1.14512042	1.40156383	0.00020873
H	-1.08280913	2.41628508	-0.00005681
O	1.18365855	2.68968784	0.00009783
H	2.03178664	3.15753912	0.00051780
O	-1.18365713	-2.68968688	-0.00009010
H	-2.03178500	-3.15753841	-0.00049373

Total Energy: E = -876.57530164

- **Tetracene:**

C	-0.00000000	0.71469879	4.88277474
C	0.00000000	1.40757715	3.70728616
C	-0.00000000	0.72483697	2.44720537
C	-0.00000000	-0.72483697	2.44720537
C	-0.00000000	-1.40757715	3.70728616
C	-0.00000000	-0.71469879	4.88277474
C	0.00000000	1.40484530	1.23392440
C	-0.00000000	-1.40484530	1.23392440
C	0.00000000	-0.72507605	0.00006507
C	0.00000000	0.72507605	0.00006507
C	0.00000000	1.40486638	-1.23413463
H	0.00000000	2.49066377	-1.23438592
C	0.00000000	0.72502870	-2.44706881
C	-0.00000000	-0.72502870	-2.44706881
C	-0.00000000	-1.40486638	-1.23413463
H	0.00000000	2.49063490	1.23453336
H	0.00000000	1.24561311	5.82805140
H	-0.00000000	2.49261116	3.70723574
H	-0.00000000	-2.49261116	3.70723574
H	-0.00000000	-1.24561311	5.82805140
H	-0.00000000	-2.49063490	1.23453336
H	-0.00000000	-2.49066377	-1.23438592
C	-0.00000000	-1.40763483	-3.70733874
C	0.00000000	1.40763483	-3.70733874
C	0.00000000	0.71474903	-4.88274235
H	0.00000000	1.24565204	-5.82802198
C	-0.00000000	-0.71474903	-4.88274235
H	-0.00000000	-1.24565204	-5.82802198
H	0.00000000	-2.49290196	-3.70723984
H	0.00000000	2.49290196	-3.70723984

Total Energy: E = -693.32921577

- **Quinacridone**

C	-3.62429700	-0.83803902	-0.00000579
C	-1.19643452	-0.73400777	-0.00002090
C	-1.22583395	0.68258504	-0.00002385
C	-2.51658090	1.41394336	-0.00004109
C	-3.72462806	0.57066926	-0.00000870
C	1.19643466	0.73400826	-0.00001641

---

C	1.22583408	-0.68258450	-0.00001737
C	2.51658063	-1.41394296	-0.00002073
C	3.72462775	-0.57066929	-0.00000147
C	3.62429725	0.83803902	-0.00000150
C	5.00008852	-1.16326297	0.00001341
C	4.79465636	1.62171597	0.00001047
C	6.14524236	-0.39101004	0.00002617
H	7.12275514	-0.85757519	0.00003659
C	6.03363952	1.01010453	0.00002399
H	6.92787710	1.62321565	0.00003388
H	5.04643267	-2.24551772	0.00001301
H	4.71538487	2.70402068	0.00001045
O	2.56223996	-2.64079082	0.00001132
C	-0.03019342	1.39594080	-0.00002018
C	0.03019361	-1.39594023	-0.00001926
C	-4.79465583	-1.62171640	0.00001169
C	-5.00008911	1.16326245	0.00001155
C	-6.03363925	-1.01010547	0.00002969
H	-6.92787652	-1.62321694	0.00004461
C	-6.14524263	0.39100904	0.00003085
H	-7.12275562	0.85757380	0.00004415
H	0.09083890	-2.47892241	-0.00001748
H	-5.04643371	2.24551717	0.00000865
H	-4.71538392	-2.70402108	0.00001398
H	-0.09083867	2.47892297	-0.00002189
N	2.38603663	1.43989790	-0.00001083
H	2.34053013	2.44748806	-0.00000994
N	-2.38603631	-1.43989737	-0.00001503
H	-2.34052960	-2.44748752	-0.00000964
O	-2.56224041	2.64079135	0.00002259

Total Energy: E = -1029.63571047

- **protonated quinacridone [quinH<sub>2</sub>]<sup>2+</sup>:**

C	3.59635459	0.87213819	-0.00000420
C	1.18438144	0.75442524	-0.00000091
C	1.23206906	-0.67365466	-0.00000417
C	2.51747299	-1.31569623	-0.00000612
C	3.70402416	-0.55774553	0.00000063
C	-1.18438142	-0.75442523	0.00000073
C	-1.23206905	0.67365467	0.00000402
C	-2.51747301	1.31569624	0.00000599
C	-3.70402416	0.55774552	-0.00000047
C	-3.59635457	-0.87213819	0.00000415
C	-5.00782539	1.13787358	-0.00001248
C	-4.75850340	-1.66854797	0.00000739
C	-6.12366834	0.34738806	-0.00000979
H	-7.10977717	0.79391219	-0.00001977
C	-5.99377850	-1.06597127	0.00000244
H	-6.88631155	-1.68053671	0.00000623
H	-5.13566039	2.21497170	-0.00002998
H	-4.67114171	-2.74920060	0.00001325
C	0.04379169	-1.41092523	-0.00000336
C	-0.04379167	1.41092524	0.00000317

---

C	4.75850344	1.66854796	-0.00000747
C	5.00782539	-1.13787359	0.00001309
C	5.99377850	1.06597125	-0.00000223
H	6.88631155	1.68053665	-0.00000605
C	6.12366834	-0.34738808	0.00001041
H	7.10977717	-0.79391221	0.00002078
H	-0.09106477	2.49259663	0.00000613
H	5.13566040	-2.21497171	0.00003111
H	4.67114175	2.74920059	-0.00001355
H	0.09106480	-2.49259662	-0.00000636
N	-2.36394880	-1.45395583	0.00000611
H	-2.32050808	-2.46668536	0.00000574
N	2.36394883	1.45395584	-0.00000634
H	2.32050811	2.46668537	-0.00000622
O	2.48021972	-2.63574265	-0.00000843
H	3.35427557	-3.05128280	-0.00005086
O	-2.48021985	2.63574267	0.00000802
H	-3.35427573	3.05128278	0.00004952

Total Energy: E = -1030.28153017

- **Pentacene:**

C	-6.11010230	0.71567839	-0.00000100
C	-4.93596792	1.40867962	-0.00000116
C	-3.67368665	0.72661557	-0.00000033
C	-3.67366671	-0.72660711	0.00000042
C	-4.93590651	-1.40870879	0.00000063
C	-6.11007118	-0.71575215	0.00000000
C	-2.46429466	1.40642453	-0.00000016
C	-2.46424028	-1.40638731	0.00000074
C	-1.22522787	-0.72749830	0.00000053
C	-1.22522328	0.72754330	0.00000032
C	0.00037036	1.40715778	0.00000052
H	-0.00045300	2.49286183	0.00000084
C	1.22442101	0.72789763	0.00000058
C	1.22434330	-0.72792432	0.00000039
C	0.00042013	-1.40711584	0.00000054
H	-2.46579844	2.49223288	-0.00000051
H	-7.05553360	1.24637807	-0.00000161
H	-4.93658221	2.49375899	-0.00000201
H	-4.93649870	-2.49378871	0.00000139
H	-7.05547761	-1.24649615	0.00000038
H	-2.46576512	-2.49219706	0.00000112
H	-0.00050116	-2.49282472	0.00000102
C	2.46502686	-1.40665569	0.00000012
C	2.46500691	1.40667046	0.00000065
C	3.67306448	0.72692253	-0.00000011
C	3.67318729	-0.72694757	-0.00000049
H	2.46548214	-2.49248980	-0.00000060
H	2.46546575	2.49249736	0.00000100
C	4.93654438	-1.40921203	-0.00000362
C	4.93647233	1.40914634	-0.00000047
C	6.10976013	0.71628660	0.00000076
H	7.05570097	1.24608177	0.00000338

---

C	6.10996265	-0.71624449	0.00000007
H	7.05600848	-1.24574349	0.00000213
H	4.93646567	-2.49473927	-0.00000096
H	4.93633196	2.49465337	0.00000093

Total Energy: E = -846.99691066

[51] Gaussian 03, Revision C.02, M. J. Frisch, G. W. Trucks, H. B. Schlegel, G. E. Scuseria, M. A. Robb, J. R. Cheeseman, J. A. Montgomery, Jr., T. Vreven, K. N. Kudin, J. C. Burant, J. M. Millam, S. S. Iyengar, J. Tomasi, V. Barone, B. Mennucci, M. Cossi, G. Scalmani, N. Rega, G. A. Petersson, H. Nakatsuji, M. Hada, M. Ehara, K. Toyota, R. Fukuda, J. Hasegawa, M. Ishida, T. Nakajima, Y. Honda, O. Kitao, H. Nakai, M. Klene, X. Li, J. E. Knox, H. P. Hratchian, J. B. Cross, V. Bakken, C. Adamo, J. Jaramillo, R. Gomperts, R. E. Stratmann, O. Yazyev, A. J. Austin, R. Cammi, C. Pomelli, J. W. Ochterski, P. Y. Ayala, K. Morokuma, G. A. Voth, P. Salvador, J. J. Dannenberg, V. G. Zakrzewski, S. Dapprich, A. D. Daniels, M. C. Strain, O. Farkas, D. K. Malick, A. D. Rabuck, K. Raghavachari, J. B. Foresman, J. V. Ortiz, Q. Cui, A. G. Baboul, S. Clifford, J. Cioslowski, B. B. Stefanov, G. Liu, A. Liashenko, P. Piskorz, I. Komaromi, R. L. Martin, D. J. Fox, T. Keith, M. A. Al-Laham, C. Y. Peng, A. Nanayakkara, M. Challacombe, P. M. W. Gill, B. Johnson, W. Chen, M. W. Wong, C. Gonzalez, and J. A. Pople, Gaussian, Inc., Wallingford CT, 2004.